# Nonlocal electron-phonon coupling of ionic charge-fluctuation type and phonon anomalies in high-temperature superconductors

Claus Falter and Georg A. Hoffmann
*Institut für Festkörpertheorie, Universität Münster, Wilhelm-Klemm-Strasse 10, 48149 Münster, Germany*
(Received 6 February 2001; published 16 July 2001)

The experimentally observed strong renormalization of the high-frequency copper-in-plane-oxygen bond-stretching vibrations in the metallic phase of $YBa_2Cu_3O_7$ and $La_2CuO_4$ is investigated. In this context the effect of the $a$-$b$ anisotropy in $YBa_2Cu_3O_7$ on these anomalous phonon modes is discussed. It is demonstrated that the characteristic softening of the modes is a generic feature of the high-temperature superconductors. It is a consequence of a strong, nonlocal electron-phonon coupling of the ionic charge-fluctuation type and not related to Fermi-surface nesting. The phase space of this strong coupling effect is shown to be large. This reveals the importance of the phonons in the mechanism leading to high-temperature superconductivity.

DOI: 10.1103/PhysRevB.64.054516 PACS number(s): 74.25.Kc, 63.20.Dj, 63.20.Kr

## I. INTRODUCTION

Inelastic neutron-scattering experiments on high-temperature superconductors (HTSC) give clear evidence of a strong electron-phonon coupling, for a review see Ref. 1. In particular, characteristic phonon anomalies generated by a large electron-lattice interaction have been detected in $La_2CuO_4$.[2–4] Here a strong softening of the high-frequency copper-in-plane-oxygen bond-stretching modes is found as holes are doped in the insulating parent compound, i.e., we have an unmistakable and important example for a direct correlation of hole doping with the phonon anomalies. The doping leads to a strong decrease of the planar oxygen breathing mode $O_B^X$ $[X=(\pi/a,\pi/a,0)$, a: lattice constant] and even more strongly for a second CuO bond-stretching vibration at wave vector $N'=(\pi/a,0,0)$, called $\Delta_1/2$ in the following.

Similar to the observations in doped $La_2CuO_4$ pronounced phonon anomalies for the Cu-in-plane-oxygen bond-stretching vibrations have also been observed by neutron-scattering experiments in $YBa_2Cu_3O_7$.[1,5] The highest $\Delta_1$ and $\Delta_4$ branches along the 100/010 direction show a strong decrease in frequency towards the zone boundary. Compared to the insulating reference compound $YBa_2Cu_3O_6$, i.e., without the characteristic electron-phonon coupling effects, there is a softening of about 5 THz. These renormalization effects observed in $YBa_2Cu_3O_7$ are qualitatively very similar to those observed in doped $La_2Cu_2O_4$ for the $\Delta_1/2$ mode. Quantitatively the effects are somewhat larger in $YBa_2Cu_3O_7$. It should be remarked that the interpretation of the measured data for the 100/010 direction in $YBa_2Cu_3O_7$ is complicated by the loss of well-defined phonon peaks about halfway to the zone boundary due to effects of twinning and possible anticrossing with other phonon branches. The presently available data that cannot distinguish between the (1,0,0) and (0,1,0) direction and their interpretation is given in Refs. 1, 5. From these experimental results it seems reasonable to assume that the anomalous phonon softening observed and correspondingly the large electron-phonon coupling is a generic feature of the HTSC.

Recently, we have studied the softening of $O_B^X$ and $\Delta_1/2$ in $La_2CuO_4$ and demonstrated that it is driven by long-ranged, nonlocal electron-phonon interaction effects of ionic charge-fluctuation (CF) type.[6,7] In the present paper we extend our calculations of the Cu-in-plane-oxygen bond-stretching anomalies to $YBa_2Cu_3O_7$ in order to clarify their physical origin in this material and compare it with the situation found in $La_2CuO_4$. Furthermore, the amount of phase space of the strong electron-phonon coupling is explored and Fermi-surface nesting as a possible scenario is discussed.

Section II presents a review of the theory and the modeling. In Sec. III the anomalous behavior of the oxygen bond-stretching modes in $La_2CuO_4$ and $YBa_2Cu_3O_7$ is calculated and shown to be generated in both materials by nonlocal electron-phonon interaction effects of ionic charge-fluctuation type. Moreover, the size of phase space for strong coupling and the effect of the $a$-$b$ anisotropy in $YBa_2Cu_3O_7$ on the anomalies is investigated. The final section presents a summary and the conclusions.

## II. THEORETICAL CONSIDERATIONS AND MODELING

A detailed description of our microscopic approach of the electronic density response, the lattice dynamics and the electron-phonon interaction (EPI) in the HTSC can be found, for example, in Refs. 8 and 9. In this formulation the local part of the electronic charge response is approximated by an *ab initio* rigid-ion model (RIM) taking into account ion softening in terms of effective ionic charges as calculated from a tight-binding analysis of the electronic band structure. In addition, scaling of the short-range part of the pair potentials between the ions is considered in order to simulate covalence effects in the calculations.[10] Scaling is performed in such a way that the energy-minimized structure is a close as possible to the experimental one. The tight-binding analysis supplies the effective ionic charges as extracted from the orbital occupation numbers $Q_\mu$ of the $\mu$ (tight-binding) orbital in question:

$$Q_\mu=\frac{2}{N}\sum_{n\mathbf{k}}|C_{\mu n}(\mathbf{k})|^2. \tag{1}$$

 

$C_{\mu n}(\mathbf{k})$ stands for the $\mu$ component of the eigenvector of band $n$ at wave the vector $\mathbf{k}$ in the first Brillouin-zone; the summation in Eq. (1) runs over all occupied states and $N$ gives the number of elementary cells in the (periodic) crystal. The rigid-ion model with the corrections just mentioned then servers as a reference system for the description of the insulating phase of HTSC. For a representation of the (nonrigid) electronic density response and screening of the HTSC, particularly in the metallic phase, more or less localized electronic CF in the outer shells of the ions are considered. The latter dominate the long-ranged, nonlocal contribution of the electronic density response and the EPI in the HTSC. In addition, dipole-fluctuations (DF) can be treated within our approach.[9] Thus, the starting point of our model are the ionic densities in the perturbed state, which are given by

$$\rho_\alpha(\mathbf{r}) = \rho_\alpha^0(r) + \sum_\lambda Q_\lambda \rho_\lambda^{\mathrm{CF}}(r) + \mathbf{p}_\alpha \cdot \hat{r} \rho_\alpha^D(r), \tag{2}$$

where $\rho_\alpha^0$ is the density of the unperturbed ion localized at the sublattice $\alpha$ of the crystal. The $Q_\lambda$ and $\rho_\lambda^{\mathrm{CF}}$ describe the amplitudes and the form factors of the charge fluctuations and the last term in Eq. (2) gives the dipolar deformation of an ion $\alpha$ with amplitude (dipole moment) $\mathbf{p}_\alpha$ and a radial density distribution $\rho_\alpha^D$. $\hat{r}$ is the unit vector in the direction of $\mathbf{r}$. The $\rho_\lambda^{\mathrm{CF}}$ are approximated by a spherical average of the orbital densities of the outer ionic shells calculated in local-density approximation (LDA) taking self-interaction effects (SIC) into account.[11] The dipole density $\rho_\alpha^D$ is obtained from a modified Sternheimer method in the framework of LDA-SIC, see Refs. 9 and 12.

The total energy of the crystal is investigated by assuming that the density of the crystal can be approximated by a superposition of overlapping densities of the individual ions $\rho_\alpha$. The $\rho_\alpha^0$ are calculated within SIC-LDA taking environment effects via a Watson sphere potential and the effective charges of the ions into account. Such an approximation holds well in the HTSC.[10,13] Moreover, applying the pair-potential approximation we get for the total energy:

$$E(R,\zeta) = \sum_{\mathbf{a}\alpha} E_\alpha^{\mathbf{a}}(\zeta) + \frac{1}{2} {\sum_{\substack{\mathbf{a}\alpha \\ \mathbf{b}\beta}}}' \phi_{\alpha\beta}(\mathbf{R}_\beta^{\mathbf{b}} - \mathbf{R}_\alpha^{\mathbf{a}}, \zeta). \tag{3}$$

The energy $E$ depends on the configuration of the ions $\{R\}$ and the electronic degrees of freedom (EDF) $\{\zeta\}$ of the charge density, i.e., $\{Q_\lambda\}$ and $\{\mathbf{p}_\alpha\}$ in Eq. (2). $E_\alpha^{\mathbf{a}}$ are the energies of the single ions. $\mathbf{a},\mathbf{b}$ denote the elementary cells in the crystal and $\alpha$, $\beta$ the sublattices. The second term in Eq. (3) is the interaction energy of the system, expressed by the pair interactions $\phi_{\alpha\beta}$. The prime in Eq. (3) means that the self-term has to be omitted. Both, $E_\alpha^{\mathbf{a}}$ and $\phi_{\alpha\beta}$ in general depend upon $\zeta$ via $\rho_\alpha$.

From the adiabatic condition

$$\frac{\partial E(R,\zeta)}{\partial \zeta} = 0, \tag{4}$$

an expression for the force constants, and accordingly, the dynamical matrix in harmonic approximation can be derived:

$$t_{ij}^{\alpha\beta}(\mathbf{q}) = [t_{ij}^{\alpha\beta}(\mathbf{q})]_{\mathrm{RIM}} - \frac{1}{\sqrt{M_\alpha M_\beta}} \sum_{\kappa,\kappa'} [B_i^{\kappa\alpha}(\mathbf{q})]^* [C^{-1}(\mathbf{q})]_{\kappa\kappa'} B_j^{\kappa'\beta}(\mathbf{q}). \tag{5}$$

$[t_{ij}^{\alpha\beta}(\mathbf{q})]_{\mathrm{RIM}}$ denotes the contribution of the RIM to the dynamical matrix. $M_\alpha, M_\beta$ are the masses of the ions and $\mathbf{q}$ is a wave vector from the first Brillouin-zone. The quantities $\mathbf{B}(\mathbf{q})$ and $C(\mathbf{q})$ represent the Fourier transforms of the coupling coefficients as calculated from the energy,

$$\mathbf{B}_{\kappa\beta}^{\mathbf{ab}} = \frac{\partial^2 E(R,\zeta)}{\partial \zeta_\kappa^{\mathbf{a}} \partial \mathbf{R}_\beta^{\mathbf{b}}}, \tag{6}$$

and

$$C_{\kappa\kappa'}^{\mathbf{ab}} = \frac{\partial^2 E(R,\zeta)}{\partial \zeta_\kappa^{\mathbf{a}} \partial \zeta_{\kappa'}^{\mathbf{b}}}. \tag{7}$$

The derivatives in Eqs. (6) and (7) have to be performed at the equilibrium positions. $\kappa$ denotes the electronic degrees of freedom (charge-fluctuations and dipole-fluctuations in the present model) in an elementary cell of the crystal. The $\mathbf{B}$ coefficients describe the coupling between the EDF and the ions and the $C$ coefficients the interaction between the EDF. The equations (5)–(7) are generally valid and, in particular, are independent of our specific model for the decomposition of the perturbed density in Eq. (2) and of the pair approximation (3) for the energy.

The pair interactions $\phi_{\alpha\beta}$ can be decomposed into long-ranged Coulomb contributions and short-ranged terms. The latter are separated into the interaction between the ion cores and the charge density from Eq. (2), the interaction between the density $\rho_\alpha$ with the density $\rho_\beta$ (Hartree contribution) and a term representing the sum of the kinetic one-particle and the exchange-correlation contribution of the interaction between the two ions. A detailed description of the $\phi_{\alpha\beta}$ and the calculation of the coupling coefficients $\mathbf{B}$ and $C$ for the EDF is given in Ref. 9. In this context it should be mentioned that the matrix $C_{\kappa\kappa'}(\mathbf{q})$ of the EDF-EDF interaction whose inverse appears in Eq. (5) for the dynamical matrix can also be written as

$$C = \Pi^{-1} + \tilde{V}. \tag{8}$$

$\Pi^{-1}$ contains the kinetic one-particle part to the interaction and $\tilde{V}$ the Hartree and exchange-correlation contribution. The quantity $C^{-1}$ needed for the calculation of the dynamical matrix is closely related to the density-response function (matrix) and to the inverse-dielectric function (matrix) $\varepsilon^{-1}$, respectively. Written in matrix notation we have the relation

$$C^{-1} = \Pi(1 + \tilde{V}\Pi)^{-1} \equiv \Pi \varepsilon^{-1}, \quad \varepsilon = 1 + \tilde{V}\Pi. \tag{9}$$

The CF-CF submatrix of the matrix $\Pi$ can be calculated approximatively from a tight-binding analysis of the (first

principles) electronic band structure. In this case the electronic polarizability $\Pi$ is given by,

$$\Pi_{\kappa\kappa'}(\mathbf{q}) = -\frac{2}{N}\sum_{\substack{n,n'\\ \mathbf{k}}} \frac{f_{n'}(\mathbf{k}+\mathbf{q}) - f_n(\mathbf{k})}{E_{n'}(\mathbf{k}+\mathbf{q}) - E_n(\mathbf{k})} [C^*_{\kappa n}(\mathbf{k}) C_{\kappa n'}(\mathbf{k} + \mathbf{q})][C^*_{\kappa' n}(\mathbf{k}) C_{\kappa' n'}(\mathbf{k}+\mathbf{q})]^*. \tag{10}$$

$f$, $E$, and $C$ are the occupation numbers, the electronic band structure, and the expansion coefficients of the Bloch functions in terms of the tight-binding functions.

The self-consistent change of the EDF $\zeta^{\mathbf{a}}_{\kappa}$ in a phonon mode $(\mathbf{q}\sigma)$ characterized by the displacements

$$\mathbf{u}^{\mathbf{a}}_{\alpha}(\mathbf{q}\sigma) = \left(\frac{\hbar}{2M_{\alpha}\omega_{\sigma}(\mathbf{q})}\right)^{1/2} \mathbf{e}^{\alpha}(\mathbf{q}\sigma) e^{i\mathbf{q}\cdot\mathbf{R}^{\mathbf{a}}} \equiv \mathbf{u}_{\alpha}(\mathbf{q}\sigma) e^{i\mathbf{q}\cdot\mathbf{R}^{\mathbf{a}}} \tag{11}$$

can be expressed in the form

$$\delta\zeta^{\mathbf{a}}_{\kappa}(\mathbf{q}\sigma) = \left[-\sum_{\alpha} \mathbf{X}^{\kappa\alpha}(\mathbf{q}) \mathbf{u}_{\alpha}(\mathbf{q}\sigma)\right] e^{i\mathbf{q}R^{\mathbf{a}}_{\kappa}} \equiv \delta\zeta_{\kappa}(\mathbf{q}\sigma) e^{i\mathbf{q}\cdot\mathbf{R}^{\mathbf{a}}}. \tag{12}$$

$\omega_{\sigma}(\mathbf{q})$ and $\mathbf{e}^{\alpha}(\mathbf{q}\sigma)$ are the phonon frequency and the polarization vector for the mode $(\mathbf{q}\sigma)$, and $\mathbf{X}^{\kappa\alpha}(\mathbf{q})$ describes the self-consistent reaction of the EDF in the phonon mode. It can be shown to be given by

$$\mathbf{X}(\mathbf{q}) = \Pi(\mathbf{q})\varepsilon^{-1}(\mathbf{q})\mathbf{B}(\mathbf{q}) = C^{-1}(\mathbf{q})\mathbf{B}(\mathbf{q}). \tag{13}$$

Finally, we introduce as a quantity, which gives the strength of the electron-phonon interaction in a certain phonon mode, namely, the change of the total self-consistent crystal potential felt by an electron, $\delta V_{\mathrm{eff}}(\mathbf{r},\mathbf{q}\sigma)$. Weighting this quantity with the corresponding density form-factor $\rho_{\kappa}(\mathbf{r}-\mathbf{R}^{\mathbf{a}}_{\kappa})$ of the EDF located at $\mathbf{R}^{\mathbf{a}}_{\kappa}$ in the crystal, we get

$$\delta V^{\mathbf{a}}_{\kappa}(\mathbf{q}\sigma) = \int dV \rho_{\kappa}(\mathbf{r}-\mathbf{R}^{\mathbf{a}}_{\kappa})\, \delta V_{\mathrm{eff}}(\mathbf{r},\mathbf{q}\sigma) \tag{14}$$

as a direct measure for the strength of electron-phonon coupling in the mode $(\mathbf{q}\sigma)$. $\delta V^{\mathbf{a}}_{\kappa}(\mathbf{q}\sigma)$ can be expressed by the coupling coefficients from Eqs. (6), (7) in the following way:

$$\delta V^{\mathbf{a}}_{\kappa}(\mathbf{q}\sigma) = \left[\sum_{\alpha} \mathbf{W}_{\kappa\alpha}(\mathbf{q}) \mathbf{u}_{\alpha}(\mathbf{q}\sigma)\right] e^{i\mathbf{q}\mathbf{R}^{\mathbf{a}}_{\kappa}} \equiv \delta V_{\kappa}(\mathbf{q}\sigma) e^{i\mathbf{q}\cdot\mathbf{R}^{\mathbf{a}}}, \tag{15}$$

where $\mathbf{W}(\mathbf{q})$ is the Fourier transform of

$$\mathbf{W}^{\mathbf{ab}}_{\kappa\beta} = \mathbf{B}^{\mathbf{ab}}_{\kappa\beta} - {}^{\mathrm{kin}}\mathbf{B}^{\mathbf{ab}}_{\kappa\beta} - \sum_{\mathbf{b}'\kappa'} \tilde{V}^{\mathbf{ab}'}_{\kappa\kappa'} \mathbf{X}^{\mathbf{b}'\mathbf{b}}_{\kappa'\beta}. \tag{16}$$

${}^{\mathrm{kin}}\mathbf{B}$ in Eq. (16) denotes the contribution of the kinetic energy to the coupling parameter $\mathbf{B}$ in Eq. (6).

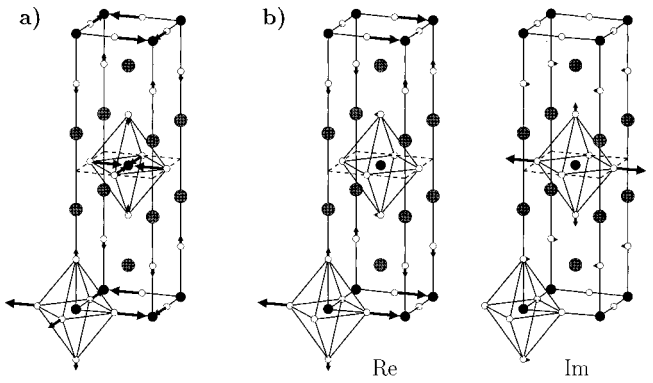


FIG. 1. Displacement pattern of the high-frequency copper-in-plane-oxygen bond-stretching vibrations of $La_2CuO_4$ (a) for $O^X_B$ and (b) for the $\Delta_1/2$ minimum. In case of $\Delta_1/2$ the real part (Re) and the imaginary part (Im) are shown.

## III. DISCUSSION OF THE PHONON ANOMALIES IN $La_2CuO_4$ AND $YBa_2Cu_3O_7$

### A. Origin of the phonon anomalies in $La_2CuO_4$

The physical origin of the strong softening of the high-frequency copper-in-plane-oxygen bond-stretching modes, called (phonon) anomalies in the following, for $La_2CuO_4$ has been discussed so far in Refs. 6 and 7. In these papers we have studied the experimentally observed phonon softening during the transition from the insulating to the metallic phase via the underdoped regime. In order to discriminate between the charge response in the insulator and the metal suitable models have been constructed being consistent with rigorous sum rules for the density response in the long-wavelength limit of the various phases. For the case of the underdoped phase a response sum-rule halfway between that of an insulator and a metal has been proposed expressing a loss in the partial density of states for the Cu $3d$ states at the Fermi level. For details of the modeling including ion softening for the ionic reference system we refer to Refs. 6 and 7.

For convenience we display in Fig. 1 the displacement patterns of the anomalies $\Delta_1/2$ and $O^X_B$. In Fig. 2 a comparison of the calculated results with the experiments[1,2,4] is shown and a good agreement is found. In particular, the increase in softening induced by the insulator-metal transition via the underdoped phase is correctly described. From our calculations in Refs. 6 and 7 for $La_2CuO_4$ it can be concluded that the phonon softening is driven by long-ranged, nonlocal electron-phonon interaction effects leading to ionic charge fluctuations on the outer shells of the ions as the dominating screening mechanism. In particular, the amplification of softening for $\Delta_1/2$ and $O^X_B$ in the optimally doped, metallic phase of $La_2CuO_4$ [full curve in Fig. 2(b)] has been explained by the growing importance of the CF in the more extended orbitals of the electronic structure. To be more specific, this additional renormalization can be related according to our calculations to the contribution of the Cu $4s$ and Cu $4p$ orbitals despite their weak accupation.[6] The physical explanation for such a behavior is related to the fact that the large on-site repulsion of the strongly localized Cu $3d$ orbital leads in tendency to a suppression of the charge fluctuations

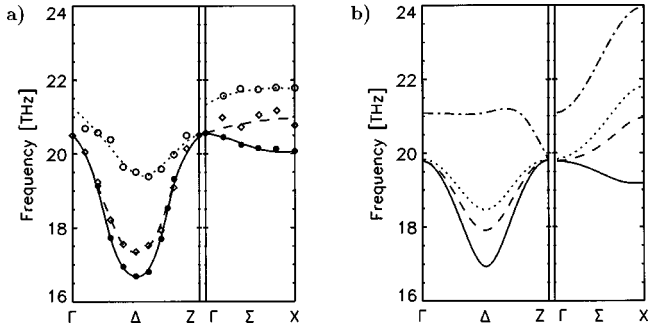


FIG. 2. (a) Experimental results for the highest $\Delta_1$ and $\Sigma_1$ branch for $La_{2-x}Sr_xCuO_4$ according to Refs. 1, 2, and 4. The open circles represent the insulating phase ($x=0$), the full circles represent the optimally doped metallic phase ($x=0.15$), and the diamonds represent the underdoped phase ($x=0.1$). The lines are a guide to the eye. (b) Calculated results for the phonon branches shown in (a) according to Ref. 7. The dotted curve gives the results for the insulating phase, the dashed curve for the underdoped phase, and the full curve for the optimally doped metallic phase. For comparison, the results of the *ab initio* rigid-ion model without any charge fluctuations (reference model for the insulating phase of the HTSC) are also displayed (dashed-dotted curve).

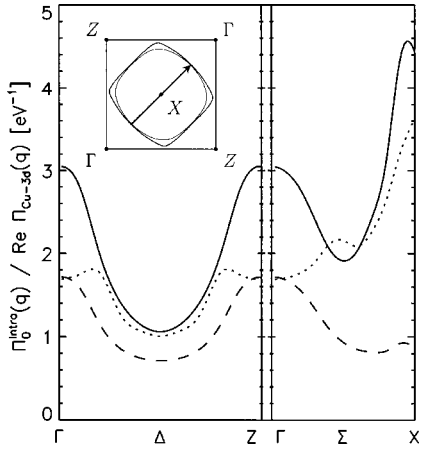


FIG. 3. Intraband contribution of the scalar electronic polarizability $\Pi_0(\mathbf{q})$, according to Eq. (17) for $La_2CuO_4$ within the 31-band model for the Fermi energy $E_F=0$ (dotted curve) and $E_F=-58$ meV (solid curve). The inset displays the nesting effect at the wave vector $X=(\pi/a)(1,1,0)$. $\Delta\sim(1,0,0)$,$\Sigma\sim(1,1,0)$. The broken lines display the dominant matrix element $\Pi_{\kappa\kappa}(\mathbf{q})$ according to Eq. (10) related to the Cu3$d$ orbital for $E_F=-58$ meV. $a$ is the lattice constant.

according to Eq. (12) via the quantity $\mathbf{X}$ or $C(\tilde{V})$, respectively, while, on the other hand, the more extended Cu 4$p$ and Cu 4$s$ orbitals, with a strongly reduced on-site repulsion, allow for an increase of the CF at the Cu ion. This, finally results in an amplification of the phonon anomalies in the optimally doped probe. Further experimental evidence other than phonons for the growing importance of the delocalized states in case of the optimally doped probe comes from optical conductivity measurements[14] that demonstrate that in the optimally doped high-$T_c$ regime an itinerant-carrier contribution develops in the conductivity spectrum.

### B. Fermi-surface nesting and phonon anomalies

In the following part we will investigate the question if Fermi-surface nesting could provide an alternative explanation for the phonon anomalies. It is well known that strong nesting at some wave vector $\mathbf{q}$ or large matrix elements at $\mathbf{q}$ or both may lead via an increased polarizability $\Pi(\mathbf{q})$ to a softening of certain phonon modes at this wave vector. A possible measure that could indicate the tendency toward such Fermi-surface driven anomalies is the scalar polarizability

$$\Pi_0(\mathbf{q})=-\frac{2}{N}\sum_{\substack{n,n'\\ \boldsymbol{\kappa}}}\frac{f_{n'}(\mathbf{k}+\mathbf{q})-f_n(\mathbf{k})}{E_{n'}(\mathbf{k}+\mathbf{q})-E_n(\mathbf{k})}. \qquad (17)$$

Our electronic structure calculations for $La_2CuO_4$ Ref. 16 used in the calculations of the polarizability rely on a tight-binding analysis of the first-principles electronic band structure as given in Ref. 15, leading altogether to an 31-band model (31 BM). This is consistent with the allowed CF for La 5$d$-, Cu 3$d$-, 4$s$-, 4$p$-, and O 2$p$-orbitals in our model. Structure in $\Pi_0$ depends mostly on parallel sheets of the Fermi surface, with a stronger nesting leading to sharper structure. The inset in Fig. 3 displays the nesting effect for the wave vector $\mathbf{q}\cong X=(\pi/a)(1,1,0)$ within the (31 BM) for the Fermi energy $E_F=0$ and $E_F=-58$ meV, respectively. The latter case corresponds in a rigid band model to optimally doped $La_2CuO_4$ where the Fermi energy lies at the van Hove singularity (VH) of the density of states. Moreover, in Fig. 3 the intraband contribution ($n=n'$) of the scalar polarizability from Eq. (17) is shown for $E_F=0$ (dotted curve) and the van Hove case (full curve). For comparison also the dominant matrix element $\Pi_{\kappa\kappa}(\mathbf{q})$ of the Cu 3$d$ orbital of the full polarizability matrix given in Eq. (10) is plotted (broken curve) for $E_F=-58$ meV. The polarizability is calculated along the $\Delta$- and $\Sigma$-direction where the phonon anomalies appear. A nesting effect in $\Pi_0(\mathbf{q})$ can only be discerned around the $X$ point. For $E_F=-58$ meV the polarizability peak is enhanced and slightly shifted away from $X$ toward $\Gamma$. On the contrary, in the middle of the $\Delta$ direction where the phonon anomalies are strongest $\Pi_0(\mathbf{q})$ approaches a minimum. Thus, there is no explanation of the strong phonon renormalization along the $\Delta$ direction by nesting of the Fermi surface. The softening of the planar-oxygen breathing mode $O_B^X$ at the $X$ point is primarily also not related to Fermi-surface nesting, because the nesting effect seen in $\Pi_0(\mathbf{q})$ is strongly suppressed by the components of the eigenvectors $C_{\kappa a}(\mathbf{k})$ contributing to the full polarizability matrix $\Pi_{\kappa\kappa'}(\mathbf{q})$ of the crystal. Such a message can be extracted from the broken curve in Fig. 3 representing the dominant matrix-element $\Pi(\mathrm{Cu}\,3d,\mathrm{Cu}\,3d)$ of $\Pi_{\kappa\kappa'}(\mathbf{q})$. The remaining matrix elements $\Pi_{\kappa\kappa'}(\mathbf{q})$ in the 31 BM are an order of magnitude smaller, which can be deduced from Fig. 4 where the real part of certain relevant matrix elements are given.

Similar conclusions as for $La_2CuO_4$ can be provided for $YBa_2Cu_3O_7$.[16] Here a tight-binding analysis according to Ref. 15 leads to a 41-band model (41 BM) and CF are allowed for Y 5$d$-, Cu 3$d$- and O 2$p$ orbitals. The Ba orbitals

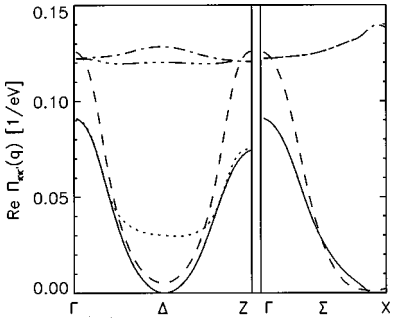


FIG. 4. Selected matrix elements of the polarizability matrix $\Pi_{\kappa\kappa'}(\mathbf{q})$ from Eq. (10) for $La_2CuO_4$ in the 31-band model. ($E_F=-58$ meV). The line types are as follows: solid line, (Cu3$d$)-($O_x2p$); dotted line, (Cu3$d$)-($O_y2p$); dashed line, ($O_x2p$)-($O_x2p$); dotted-dashed line, ($O_x2p$)-($O_y2p$); dotted-dotted-dotted-dashed line, ($O_y2p$)-($O_y2p$).

are neglected in this tight-binding fit. As already remarked strong phonon anomalies corresponding to the $\Delta_1/2$ anomaly in $La_2CuO_4$ are observed at the $X=(\pi/a,0,0)$ and $Y=(0,\pi/b,0)$ point in $YBa_2Cu_3O_7$ that cannot be untied experimentally because of twinning and possible anticrossing with other branches. In order to test if nesting plays a role for these anomalies we have calculated along the relevant symmetry directions $\Sigma\sim(1,0,0)$, $\Delta\sim(0,1,0)$ and along $\Gamma-S(S\approx(\pi/a,\pi/b,0))$ the contribution to $\Pi_0(\mathbf{q})$ from four bands of the band structure around the Fermi surface. The result is presented in Fig. 5. In particular at $X$, $Y$, and $S$ minima appear in the polarizability, i.e., there is no indication that nesting may be the source for the anomalies.

From our findings we conclude that the phonon anomalies and the strong electron-phonon coupling can be understood in a local picture in terms of nonlocally excited CF in the outer shells of the ions, which are controlled by the kinetic one-particle contribution $\Pi^{-1}$ to the electronic coupling coefficient $C$ in Eq. (8) together with the contribution of the potential energy $\tilde{V}$, i.e., the Hartree- and exchange-correlation part of $C$. In this context we realize that the interplay between strong correlation effects related to the localized Cu 3$d$ orbitals with their tendency to suppress the ionic CF with low energy via $\tilde{V}$ (the calculated on-site repulsion in units of $e^2/a_B$ for Cu 3$d$ has the large value of 1.005) and the contribution of the more extended orbitals (O 2$p$, Cu 4$s$, Cu 4$p$ with a smaller calculated on-site repulsion: 0.671, 0.356, 0.279) which tend to enhance the CF is an essential feature for an understanding of the charge response in a quantitive manner and of its influence on the phonons.

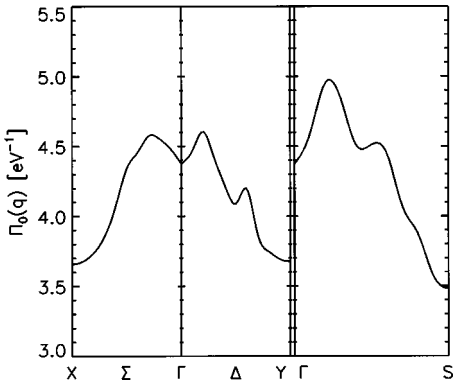


FIG. 5. Scalar electronic polarizability $\Pi_0(\mathbf{q})$ from Eq. (17) for $YBa_2Cu_3O_7$ within the 41-band model. In the figure the contribution to $\Pi_0(\mathbf{q})$ from the four bands (33–36) around the Fermi level is displayed. $\Sigma\sim(1,0,0)$, $\Delta\sim(0,1,0)$, $(\Gamma-S)\sim(1,1,0)$, $X=(\pi/a)\times(1,0,0)$, $Y=\pi/b(0,1,0)$, $S=(\pi/a,\pi/b,0)$. $a$, $b$ are lattice constants.

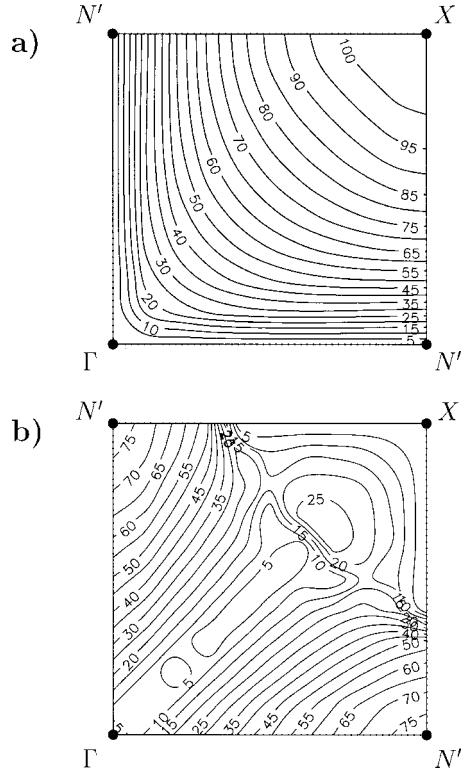


FIG. 6. Phonon-induced changes of the crystal potential (in meV) $\delta V_\kappa(\mathbf{q}\sigma)$ of $La_2CuO_4$ from Eqs. (14–16) for the dominant Cu3$d$ orbital in the $q_z=0$ plane. In (a) the result for the highest phonon branch with the $O_B^X$ anomaly at the $X$ point is given and in (b) the result for the second highest branch with the $\Delta_1/2$ anomaly at $N'=(\pi/a)(1,0,0)$, is given. See also Fig. 7.

### C. On the size of phase space for strong nonlocal electron-phonon coupling

We now explore, using $La_2CuO_4$ as an example, the size of phase space where strong nonlocal electron-phonon coupling of ionic origin appears. We will show that the strong coupling effects leading to the phonon anomalies are not restricted to a small portion of the Brillouin zone but extend to a large part. As a measure for the electron-phonon coupling strength we apply the phonon-induced changes of the self-consistent crystal potential $\delta V_\kappa(\mathbf{q}\sigma)$ defined in Eqs. (14)–(16).

The result for $\delta V_\kappa(\mathbf{q}\sigma)$ is shown in Fig. 6 in the $q_z=0$ plane of the Brillouin zone for the Cu 3$d$ orbital being most important. In part (a) of the figure the data for $\delta V_\kappa$ of the phonon branch with the highest frequency in the spectrum is

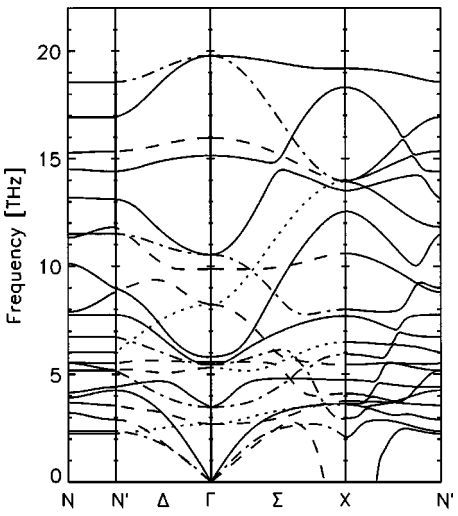


FIG. 7. Calculated phonon dispersion for $La_2CuO_4$ along the directions $\Delta\sim(1,0,0)$, $\Sigma\sim(1,1,0)$, $(X\text{-}N')$, and $(N'\text{-}N)$. $N'=(\pi/a)(1,0,0)$, $N=(\pi/a,0,\pi/c)$. The results have been obtained with the model proposed in Ref. 7 for the description of the optimally doped metallic phase. See also the full curves in Fig. 2(b).

given with the $O_B^X$ anomaly at the $X=(\pi/a)(1,1,0)$ point. Part (b) displays the result for $\delta V_\kappa$ of the second highest branch with the $\Delta_1/2$ anomaly at $N'=(\pi/a)(1,0,0)$. For example, we obtain for the magnitude of $\delta V_\kappa$ for the Cu $3d$ orbital in the $O_B^X$ mode 104.70 meV and in the $\Delta_1/2$ anomaly 77.85 meV, respectively. $\delta V_\kappa$ is vanishing for symmetry reasons for the O $2p$ orbital in $O_B^X$ while in the $\Delta_1/2$ anomaly we get a value of 8.09 meV. The calculation demonstrates that in a large part of the zone around the $O_B^X$ and the $\Delta_1/2$ anomaly strong phonon-induced changes in the potential can be found. In Fig. 7 the complete calculated phonon dispersion of $La_2CuO_4$ is displayed along the symmetry directions $\Delta\sim(1,0,0)$, $\Sigma\sim(1,1,0)$, and for $X$ to $N'$ and $N'$ to $N=(\pi/a,0,\pi/c)$. In the latter direction, i.e., perpendicular to the $q_z=0$ plane in $c$ direction, the anomalous modes practically have no dispersion. This means that the strong coupling also extends to the $q_z$ direction of the BZ. Moreover, from the shape of the experimentally observed $\Delta_1$ branch in Fig. 2(a) that displays a broader minimum as compared with the theoretical results in Fig. 2(b) it can be concluded that the phase space of strong coupling is even larger than predicted by the calculations.

Concerning the unstable phonon branch in $\Sigma$ direction in Fig. 7 it should be remarked that this branch corresponds at the $X$ point to the tilt mode and the instability of this mode announces correctly the phase transition from the tetragonal to the low-temperature orthorhombic structure.

Summarizing this section we find a large phase space for strong nonlocal electron-phonon coupling of ionic CF-type related to the high-frequency oxygen modes. This adds weight to the importance of the EPI in the pairing mechanism of the HTSC in general. Such a generalization to other HTSC is supported by the investigation of the phonon anomalies for $YBa_2Cu_3O_7$ that will be done in the following part.

### D. Phonon anomalies and *a-b* anisotropy in $YBa_2Cu_3O_7$ and the oxygen chain mode

A tight-binding analysis of the 41 BM yields reduced effective ionic charges for those sublattices, which have been considered in the tight-binding band structure of Ref. 15. We obtain the following charges as an expression of the mixed ionic-covalent bonding in $YBa_2Cu_3O_7$:Y(+2.38), Ba(+2.00), Cu1(+1.98), Cu2(+1.61), O1(−1.52), O2(−1.55), O3(−1.60), O4(−1.88). Cu1 and O1 belong to the chain, Cu2, O2, O3 to the plane and O4 is the apex oxygen.

Performing in addition covalent scaling of the short range part of the pair-potentials for the Cu-O pairs, we get the structural parameters for $YBa_2Cu_3O_7$ characterized as model $M1$ in Table I. These parameters, exept for Ba, differ at most by about 2.5% from the experimental data. The relative position for Ba is overestimated by about 7%. Notice, that Ba was not considered in the tight-binding fit of the band structure and has been assumed to be fully ionic. It is possible to improve the results for the structure and for the phonon dispersion by allowing for ion softening of the Ba ion too. This has been achieved in the model $M2$ of Table I, which considerably improves the Ba position. The corresponding effective ionic charges for $M2$ are: Y(+2.28), Ba(+1.70), Cu1(+1.98), Cu2(+1.61), O1(−1.52), O2(−1.40), O3(−1.40), O4(−1.88).

We now investigate the renormalization of the phonon dispersion along the $\Sigma\sim(1,0,0)$, $\Delta\sim(0,1,0)$, and $\Gamma\sim S\sim(1,1,0)$ direction for the highest phonon branches of symmetry-type 1 and 2 in our notation, which are associated with the planar Cu-O2/3 bond-stretching vibrations (note $\Delta_2$ in our notation corresponds to $\Delta_4$ in the notation of Refs. 1 and 5). In Fig. 8 the displacement patterns of the oxygen bond-stretching modes are shown at the symmetry points $\Gamma=(0,0,0)$, $X=(\pi/a,0,0)$, $Y=(0,\pi/b,0)$ and $S=(\pi/a,\pi/b,0)$. Moreover, the O1-chain modes $B_{2u}^\Gamma$ and $B_{2u}^X$ polarized in the $y$ direction at $\Gamma$ and $X$ are displayed, see the

TABLE I. Structural parameters for $YBa_2Cu_3O_7$ for the models $M1$ and $M2$ as defined in the text. The lattice constants $a$, $b$, $c$ are in units of Å and the internal positions of the ions in units of $c$. The experimental results (Exp) are from Ref. 17.

| | $a$ | $b$ | $c$ | $z$(Ba) | $z$(Cu2) | $z$(O2) | $z$(O3) | $z$(O4) |
|---|---|---|---|---|---|---|---|---|
| $M1$ | 3.779 | 4.031 | 11.854 | 0.1966 | 0.3498 | 0.3875 | 0.3740 | 0.1576 |
| $M2$ | 3.837 | 4.030 | 12.388 | 0.1842 | 0.3412 | 0.3942 | 0.3813 | 0.1613 |
| Exp | 3.814 | 3.885 | 11.660 | 0.1843 | 0.3546 | 0.3781 | 0.3777 | 0.1572 |

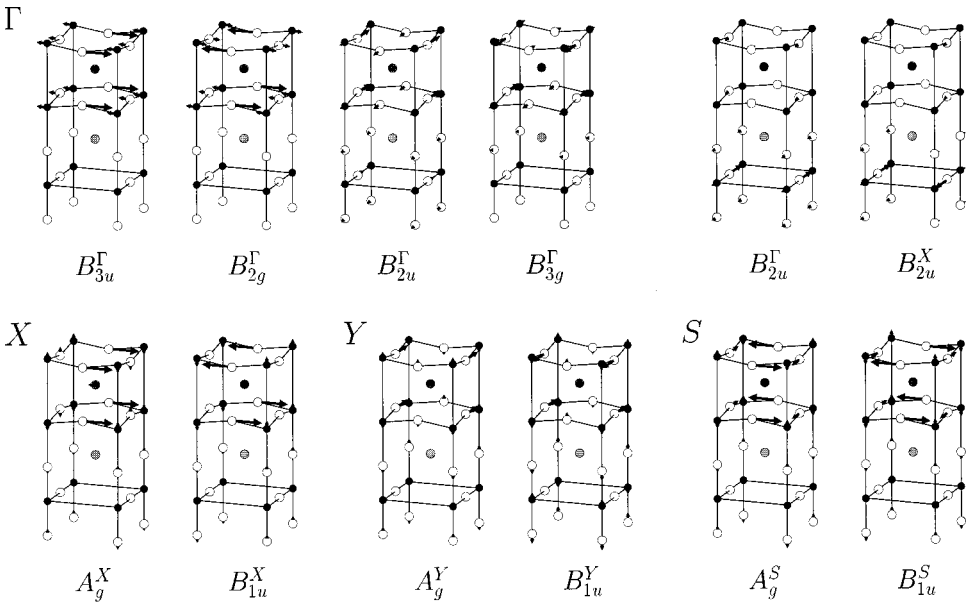


FIG. 8. Displacement patterns of the oxygen bond-stretching modes at the high-symmetry points $\Gamma=(0,0,0)$, $X=(\pi/a)\times(1,0,0)$, $Y=(\pi/b)(0,1,0)$, and $S=(\pi/a,\pi/b,0)$. In addition to the upper right, the O1-chain modes $B_{2u}^{\Gamma}$ and $B_{2u}^{X}$ polarized in the *y* direction are shown.

two patterns to the upper right of Fig. 8. The *S* point modes are oxygen breathing modes where the two types of vibrations, $A_g^s$ and $B_{1u}^s$, are distinguished from each other by the relative phase of the elongations in the two CuO planes. At *X* and *Y*, respectively, only one oxygen sublattice O2 or O3 is vibrating along the Cu-O bonding axis. The vibrations are in phase for $A_g^{x,y}$ and in opposite phase for $B_{1u}^{x,y}$ with respect to the two CuO planes. At the Γ point these modes essentially show the same behavior as the corresponding modes at the zone boundary.

On account of the *a*-*b*-anisotropy the *x*- and *y*-polarized modes $(B_{3u}^{\Gamma},B_{2g}^{\Gamma})$ and $(B_{2u}^{\Gamma},B_{3g}^{\Gamma})$, respectively, have different frequencies. According to recent neutron measurements[1,18] the mode splitting between $B_{3u}^{\Gamma}$ and $B_{2u}^{\Gamma}$ associated with this anisotropy is about 1.4 THz that is close to the splitting between $B_{2g}^{\Gamma}$ and $B_{3g}^{\Gamma}$ (1.6 THz) measured by Raman spectroscopy.[19]

As the reference model to calculate the phonon anomalies we use the model $M2$ allowing in addition for dipole-fluctuations on the ions in *z* direction (model $M3$ in the following). These fluctuations have been calculated according to a modified Sternheimer method in the framework of the local-density approximation taking self-interaction effects into account, see Ref. 9 for details. Dipole fluctuations in *x*- or *y*-direction have been neglected. In the CuO planes they are strongly screened and in the ionic layers the *z* dipoles have been found to be most important.[20] Charge fluctuations as the dominating screening mechanism in the HTSC are taken into account within the 41 BM, i.e., for the Y $5d$, Cu $3d$ and O $2p$ orbitals. Detailed calculations of the full phonon dispersion in the symmetry directions $\Delta,\Sigma(\Gamma-S)$ using such a model have been performed in Ref. 16. For our purpose here, to study the oxygen bond-stretching anomalies, we propose similarly as in Ref. 7 for $La_2CuO_4$, a simpler diagonal model independent of the wave vector $\mathbf{q}$ for the polarizability matrix $\Pi_{\kappa\kappa'}(\mathbf{q})$ from Eq. (10). Accordingly we approximate $\Pi_{\kappa\kappa'}(\mathbf{q})$ by a diagonal matrix where the diagonal elements are obtained from the partial densities of states at the Fermi level $E_F$

$$Z_\kappa(E_F)=\frac{2}{N}\sum_{n\mathbf{k}}\ \delta(E_n(\mathbf{k})-E_F)C_{\kappa n}^{\mathrm{eff}}(\mathbf{k}), \tag{18}$$

$$C_{\kappa n}^{\mathrm{eff}}(\mathbf{k})=\sum_{\mu\in\kappa}\ |C_{\mu n}(\mathbf{k})|^2. \tag{19}$$

In Eq. (19) the tight-binding orbitals related to a certain angular quantum number are summed up to an effective orbital number $\kappa$. The total density of states at the Fermi level is given in this representation by

$$Z(E_F)=\sum_{\kappa}\ Z_\kappa(E_F). \tag{20}$$

The $Z_\kappa(E_F)$ have been calculated from the 41 BM of the electronic band structure. Finally, we obtain in units of $(\mathrm{eV})^{-1}$:

$$\Pi(\mathrm{Y})=0.024,\quad \Pi(\mathrm{Cu1})=0.502,\quad \Pi(\mathrm{Cu2})=0.401,$$

$$\Pi(\mathrm{O1})=0.211,\quad \Pi(\mathrm{O2})=0.629,$$

$$\Pi(\mathrm{O3})=0.381,\quad \Pi(\mathrm{O4})=0.411.$$

Calculating the phonon dispersion with such a model $(M4)$ produces only small differences in comparison with the full 41 BM. In particular the phonon anomalies are represented very well by this model, the deviations are less than 0.1 THz.[16]

Motivated by our findings concerning the amplification of the phonon anomalies in $La_2CuO_4$ by the growing importance of the CF in the more extended $4s$ and $4p$ orbitals of the Cu ion, which are not considered in the tight-binding fit of Ref. 15 leading to the 41 BM or the simplified model $M4$, respectively, we propose another model $(M5)$. Additionally to the orbital polarizabilities defining $M4$ we assume in $M5$ small on-site polarizabilities for Cu $4s$ and Cu $4p$ orbitals:

$$\Pi(\mathrm{Cu2}\ 4s)=\Pi(\mathrm{Cu2}\ 4p)=0.025(\mathrm{eV})^{-1}.$$

TABLE II. Frequencies in THz of the oxygen bond-stretching modes of $YBa_2Cu_3O_7$ at the points of symmetry *X*, *Y*, and *S* (see Fig. 8). The models *M*3, *M*4, *M*5 are defined in the text. $X=(\pi/a,0,0)$, $Y=(0,\pi.b,0)$, $S=(\pi/a,\pi/b,0)$.

| | *M*3 | *M*4 | *M*5 |
|---|---|---|---|
| $X\ A_g$ | 22.27 | 20.27 | 19.77 |
| $B_{1u}$ | 20.60 | 19.38 | 18.95 |
| $Y\ A_g$ | 20.59 | 17.71 | 17.15 |
| $B_{1u}$ | 18.73 | 17.19 | 16.67 |
| $S\ A_g$ | 23.55 | 21.84 | 20.84 |
| $B_{1u}$ | 22.21 | 20.80 | 20.03 |

A comparison of the calculated results for the models *M*4 and *M*5 including CF with the model *M*3 without CF is given in Table II for the phonon anomalies at *X*, *Y*, and *S*. The data clearly demonstrate the importance of the nonlocally induced CF for the decrease in frequency of the oxygen bond-stretching modes. For example $A_g^x$ is renormalized by 2.5 THz from 22.27 THz in *M*3 to 19.77 THz in *M*5 or $A_g^y$ by 3.44 THz from 20.59 THz to 17.15 THz, etc. In the experiments because of effects of twinning it cannot be distinguished between the *X* and *Y* point. As a consequence, the experimentally reported phonon softening of about 5 THz Refs. 1, 5, and 18 when going from $\Gamma$ to *X*/*Y* has to be related to the calculated difference in frequency ($\Delta_{\rm ano}$) between $B_{3u}^{\Gamma}$ (highest mode) and the $B_{1u}^{Y}$ (lowest mode). From Table II and III we extract $\Delta_{\rm ano}=4.61$ THz for *M*4 and $\Delta_{\rm ano}=5.13$ THz for *M*5, respectively. Thus, the magnitude of the anomaly is in a good agreement with the experiments, in particular for *M*5. Comparing to the situation in $La_2CuO_4$ we get in $YBa_2Cu_3O_7$ a doubling of the anomalous oxygen bond-stretching modes with strong nonlocal coupling in a large part of the Brillouin zone.

The full dispersion curves with the anomalously renormalized oxygen bond-stretching modes, marked by the open circles at *X*, *Y*, and *S*, are shown in Figs. 9(a) and 9(b) for the models *M*4 and *M*5. The line types in the figure denote the corresponding irreducible representations (ID) of the small point group of the wave vector **q** (ID) 1 corresponds to the full curves, ID 2 to the dotted curves, ID 3 to the broken curves, and ID 4 to the dash-dotted curves. We extract that the effect of the CF in the more extended orbitals, taken into account in *M*5, enhances the phonon anomalies, similarly as found for $La_2CuO_4$.

TABLE III. Frequencies in THz of the oxygen bond-stretching modes $B_{3u}^{\Gamma}, B_{2g}^{\Gamma}, B_{2u}^{\Gamma}, B_{3g}^{\Gamma}$ and of the chain mode $B_{2u}^{\Gamma}$ in the last column (see also Fig. 8) dependent on the magnitude of the covalent scaling parameter $R_c^0[a_B]$ for the Cu1-O1 bond. The first row represents the results for the models *M*4 and *M*5. The results in the second and third row have been obtained by assuming a smaller covalency ($R_c^0=-0.1$) and a larger covalency ($R_c^0=-0.18$), respectively. The results for *M*4 and *M*5 are the same because charge fluctuations are not excited in these modes for symmetry reasons, only the LO-TO splits are closed in the odd modes ($B_{2u}^{\Gamma}, B_{3u}^{\Gamma}$).

| $R_c^0$ | $B_{3u}^{\Gamma}$ | $B_{2g}^{\Gamma}$ | $B_{2u}^{\Gamma}$ | $B_{3g}^{\Gamma}$ | $B_{2u}^{\Gamma}$ |
|---|---|---|---|---|---|
| −0.1474 | 21.80 | 21.24 | 19.43 | 18.88 | 19.03 |
| −0.10 | 21.41 | 20.86 | 19.09 | 18.50 | 19.66 |
| −0.18 | 21.56 | 21.01 | 19.52 | 18.94 | 17.98 |

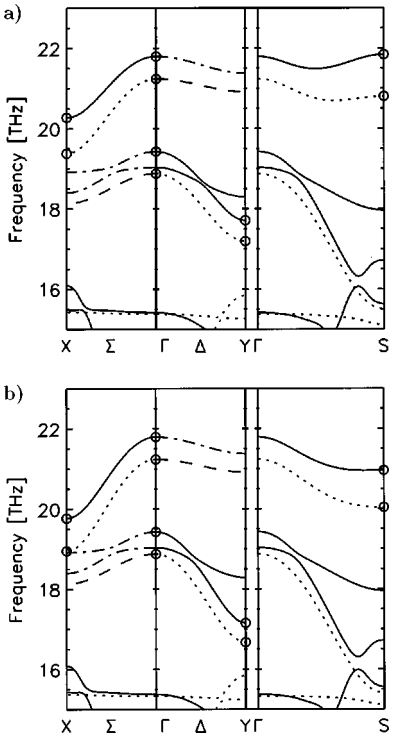


FIG. 9. Calculated phonon dispersion curves of $YBa_2Cu_3O_7$ according to the models *M*4 (a) and *M*5 (b) as explained in the text. The anomalous oxygen bond-stretching modes are marked by open circles at *X*, *Y*, and *S*. The line types correspond to the different irreducible representations that characterize the modes 1, solid; 2, dotted; 3, dashed; 4, dotted-dashed.

The calculated *a*-*b*-anisotropy $\Delta_u \equiv \nu(B_{3u}^{\Gamma}) - \nu(B_{2u}^{\Gamma})$ and $\Delta_g \equiv \nu(B_{2g}^{\Gamma}) - \nu(B_{3g}^{\Gamma})$ can be read off from Table III as about 2.4 THz. This overestimates the experimental results $\Delta_u = 1.4$ THz and $\Delta_g = 1.6$ THz. We further have investigated this anisotropy effect on the phonons[16] and found that it depends crucially on the bonding in the CuO chain. We have simulated different degrees of covalency of the Cu1-O1 bond in our modeling by choosing the covalent scaling parameter $R_c^0$(Cu1-O1) of that bond in one way or the other. Assuming a moderate degree of covalent bonding ($R_c^0=-0.1a_B$) and determining the remaining Cu-O scaling parameters by free variation according to the scaling procedure for the energy[10] we obtain the results listed in the second row of Table III. The anisotropy splitting is nearly the same as for *M*4 and *M*5 in this case. On the other hand, if the covalent character of the Cu1-O1 bond is increased ($R_c^0=-0.18a_B$, see Table III) the *a*-*b*-anisotropy is reduced to about 2 THz. This is in better agreement with the experiment and points to the importance of covalency for the copper-oxygen bonding in the chain.

Figure 10 displays the calculated phonon dispersion for the two cases just discussed. The less covalent situation is

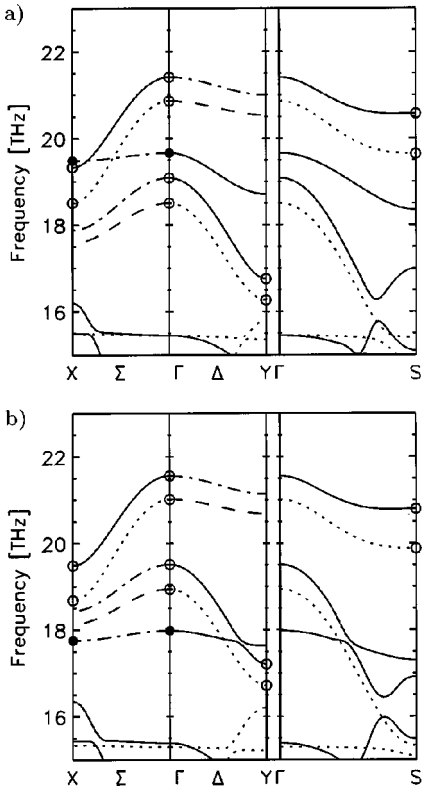


FIG. 10. Calculated phonon dispersion of $YBa_2Cu_3O_7$ dependent on the covalency of the Cu1-O1 bond characterized by the scaling parameter $R_c^0$. (a) $R_c^0=-0.1a_B$, (b) $R_c^0=-0.18a_B$. The planar oxygen bond-stretching modes at the symmetry points are marked by open circles and the oxygen chain mode are marked by full circles. The line types of the branches are as in Fig. 9.

shown in Fig. 10(a) and the more covalent one in Fig. 10(b). The anomalous planar bond-stretching modes at *X*, *Y*, and *S* are only weakly influenced (open circles). However, the O1 modes polarized in *y* direction corresponding to the nearly dispersionless branch of $\Sigma_4$ symmetry (full circles at $\Gamma$ and *X*) are strongly varied with the covalency of the Cu1-O1 bond. Both, at $\Gamma$ and at *X* the O1 ions are vibrating with large amplitude along the chain direction, see Fig. 8. This oxygen chain mode has not been detected in the neutron experiments till now[18] and our modeling could give some hints where in the spectrum one should look for this mode. In case of a moderate covalent bonding this mode is predicted in the frequency range of the two anomalous branches starting at $B_{3u}^{\Gamma}$ and $B_{2u}^{\Gamma}$, see Fig. 10(a). Increasing the covalency in the Cu1-O1 bond the chain mode is shifted to lower frequencies [Fig. 10(b)]. Simultaneously we observe in the $\Delta$ direction an anticrossing of the two highest $\Delta_1$ branches. Such a feature together with effects of twinning might lead in the experiments to the observed loss of well-defined phonon peaks in part of the Brillouin-zone. Differently spoken, the existence of anticrossing points to a strong covalency of the Cu-O bond in the chain and consequently the chain mode should exist in the frequency range of the anticrossing effect. For completeness we add that in case of nearly ionic forces assumed for the Cu1-O1 bond ($R_c^0=-0.05a_B$) the chain mode becomes the highest mode in the spectrum and the *a*-*b*-anisotropy splitting is clearly overestimated ($\Delta_{u/g}\equiv 5$ THz). This means that a weakly covalent Cu1-O1 bond can be ruled out.

## IV. SUMMARY AND CONCLUSIONS

Our calculations have shown that the experimentally observed anomalous softening of the planar oxygen bond-stretching modes in $La_2CuO_4$ and $YBa_2Cu_3O_7$ is due to nonlocal electron-phonon interaction effects of the ionic charge-fluctuation type. These results point to a common origin of the anomalies and to their existence in the other HTSC as well. The nonlocal coupling effects, not present in conventional metals and superconductors, are typical for the HTSC because of their ionic nature favoring localized intracell charge fluctuations. An enhancement of softening in the optimally doped metallic phase of the HTSC has been shown to be related to the growing importance of the charge fluctuations in the more extended orbitals of the electronic structure, in spite of their weak occupation. In $YBa_2Cu_3O_7$ a doubling of the strongly coupling anomalous oxygen bond-stretching modes is obtained as compared to $La_2CuO_4$.

The investigation of the electronic polarizability for $La_2CuO_4$ and $YBa_2Cu_3O_7$ indicates that Fermi-surface nesting is not the source of the phonon anomalies. Using $La_2CuO_4$ as an example, we realize that the size of phase space for the strong nonlocal coupling effects in the oxygen bond-stretching vibrations extends to a large part of the Brillouin zone. From these findings it can be concluded that nonlocal electron-phonon coupling of ionic CF type is an important ingredient of the pairing mechanism in the HTSC. More general, our calculations point to the fact that materials that reconcile strong bonding characterized by a dominating ionic component with metallic properties are promising candidates for high-$T_c$ materials via the nonlocal electron-phonon mechanism. This conclusion is additionally supported by the calculations in Ref. 21 where it is shown, that in a small cone around the *c* axis a nonlocal, nonadiabatic *insulatorlike* out-of-plane charge response exists, which leads to strong coupling effects for the electrons in the CuO plane providing a favorable situation for pairing. Furthermore, as far as the planar oxygen bond-stretching modes are concerned, there is also evidence for the importance of their contribution to Cooper pairing from tunneling spectroscopy on $Bi_2Sr_2CaCu_2O_8$.[22–24]

The physical picture of pairing that arises from the nonlocal EPI effects found to be important for the HTSC by our calculations (which neglect spin fluctuations) is the following: The first electron of the pair generates an excited system composed of atomic displacements and localized ionic charge fluctuations while the second electron of the pair, retarded in time, is attracted by this formerly excited system consisting of coupled lattice and charge degrees of freedom. Relevant phonon modes for this coupling mechanism are the Cu-in-plane-oxygen bond-stretching modes studied in this paper, which can be treated in adiabatic approximation and, as discussed in Ref. 21 for $La_2CuO_4$, modes from the nonadiabatic cone around the *c* axis like the axial oxygen and the axial lanthanum breathing mode at the *Z* point.

Discussing the experimentally observed large phonon-anomalies in $YBa_2Cu_3O_7$ in addition to the effect of the CF the *a-b*-anisotropy of this material must be taken into account. The anisotropy is influenced in a sensitive way by the degree of covalence of the Cu1-O1 bond.

Finally, we have investigated the position of the oxygen chain mode in the spectrum in dependence of the covalency of this bond. The latter mode has not been found in the experiments up to the present.

## ACKNOWLEDGMENT

We greatly appreciate the financial support by the Deutsche Forschungsgemeinschaft.

[1] L. Pintschovius and W. Reichardt, in *Neutron Scattering in Layered Copper-Oxide Superconductors*, edited by A. Furrer, Physics and Chemistry of Materials with Low Dimensional Structures, Vol. 20 (Kluwer Academic, Dordrecht, 1998), p. 165.
[2] L. Pintschovius and M. Braden, J. Low Temp. Phys. **105**, 813 (1996).
[3] R. J. Mc Queeney, Y. Petrov, T. Egami, M. Yethiray, G. Shirane, and Y. Endoh, Phys. Rev. Lett. **82**, 628 (1999).
[4] L. Pintschovius and M. Braden, Phys. Rev. B **60**, R15 039 (1999).
[5] W. Reichardt, J. Low Temp. Phys. **105**, 807 (1996).
[6] C. Falter, M. Klenner, G. A. Hoffmann, and Q. Chen, Phys. Rev. B **55**, 3308 (1997).
[7] C. Falter and G. A. Hoffmann, Phys. Rev. B **61**, 14 537 (2000).
[8] C. Falter, M. Klenner, and W. Ludwig, Phys. Rev. B **47**, 5390 (1993).
[9] C. Falter, M. Klenner, G. A. Hoffmann, and F. Schnetgöke, Phys. Rev. B **60**, 12 051 (1999).
[10] C. Falter, M. Klenner, and G. A. Hoffmann, Phys. Rev. B **52**, 3702 (1995).
[11] J. P. Perdew and A. Zunger, Phys. Rev. B **23**, 5048 (1981).
[12] G. D. Mahan and R. K. Subbaswamy, *Local Density Theory of Polarisability* (Plenum, New York, 1990).
[13] H. Krakauer, W. E. Pickett, and R. E. Cohen, J. Supercond. **1**, 111 (1988).
[14] S. Uchida, T. Ido, H. Tagaki, T. Arima, Y. Tokura, and S. Tajima, Phys. Rev. B **43**, 7942 (1991).
[15] M. J. De Weert, D. A. Papaconstantopoulos, and W. E. Pickett, Phys. Rev. B **39**, 4235 (1989).
[16] G. A. Hoffmann, Ph.D. thesis, University of Münster, 2000.
[17] R. J. Cava, A. W. Hewat, E. A. Hewat, B. Batlogg, M. Marezio, K. M. Rabe, J. J. Krajewski, W. F. Peck, Jr., and L. W. Rupp, Jr., Physica C **165**, 419 (1990).
[18] L. Pintschovius (private communication).
[19] K. F. McCarty, J. Z. Liu, R. N. Shelton, and H. B. Radkovsky, Phys. Rev. B **41**, 8792 (1990).
[20] F. Schnetgöke (private communication).
[21] C. Falter, M. Klenner, and G. A. Hoffmann, Phys. Rev. B **57**, 14 444 (1998).
[22] R. Aoki and H. Murakami, J. Low Temp. Phys. **105**, 1231 (1996).
[23] R. Aoki, H. Murakami, T. Kita, M. Shirai, Y. Nishio, V. M. Svistanov, A. I. Dyachenko, and D. N. Afanassyev, Physica B **219–220**, 172 (1996).
[24] R. Aoki, H. Murakami, M. Shirai, V. M. Svistunov, and D. N. Afanassyev, Physica C **282–287**, 979 (1997).